Title
Emergent behavior of LaNiO3 in short-periodic nickelate superlattices

Journal
APL Materials, 8(4)

ISSN
2166-532X

Authors
Patel, Ranjan Kumar
Meyers, D
Liu, Xiaoran
et al.

Publication Date
2020-04-01

DOI
10.1063/5.0004530

Peer reviewed

APL Materials

Emergent behavior of $LaNiO_3$ in short-periodic nickelate superlattices

Cite as: APL Mater. **8**, 041113 (2020); https://doi.org/10.1063/5.0004530
Submitted: 11 February 2020 . Accepted: 02 April 2020 . Published Online: 17 April 2020

Ranjan Kumar Patel, D. Meyers, Xiaoran Liu, Prithwijit Mandal, M. Kareev, P. Shafer, J.-W. Kim, P. J. Ryan, S. Middey, and J. Chakhalian

Emergent behavior of $LaNiO_3$ in short-periodic nickelate superlattices

Cite as: APL Mater. 8, 041113 (2020); doi: 10.1063/5.0004530
Submitted: 11 February 2020 • Accepted: 2 April 2020 •
Published Online: 17 April 2020

Ranjan Kumar Patel,[1] D. Meyers,[2] Xiaoran Liu,[3] Prithwijit Mandal,[1] M. Kareev,[3] P. Shafer,[4] J.-W. Kim,[5] P. J. Ryan,[5] S. Middey,[1,a)] and J. Chakhalian[3]

AFFILIATIONS

[1]Department of Physics, Indian Institute of Science, Bengaluru 560012, India
[2]Department of Physics, Oklahoma State University, Stillwater, Oklahoma 74078, USA
[3]Department of Physics and Astronomy, Rutgers University, Piscataway, New Jersey 08854, USA
[4]Advanced Light Source, Lawrence Berkeley National Laboratory, Berkeley, California 94720, USA
[5]Advanced Photon Source, Argonne National Laboratory, Argonne, Illinois 60439, USA

[a)]**Author to whom correspondence should be addressed:** smiddey@iisc.ac.in

ABSTRACT

Heterostructure engineering provides an efficient way to obtain several emergent phases of $LaNiO_3$, as demonstrated in recent studies. In this work, a new class of short-periodic superlattice, consisting of $LaNiO_3$ and $EuNiO_3$, has been grown by pulsed laser interval deposition to investigate the effect of structural symmetry mismatch on the electronic and magnetic behaviors. Using synchrotron-based soft and hard x-ray resonant scattering experiments, we have found that these heterostructures undergo simultaneous electronic and magnetic transitions. Most importantly, $LaNiO_3$ within these artificial structures exhibits a new antiferromagnetic, charge ordered insulating phase, which may be a potential candidate to achieve high temperature superconductivity.

The prediction of achieving high T_c superconductivity in $LaNiO_3$ through interface and orbital engineering has led to remarkable progress over the last 10 years in the synthesis and characterization of $RENiO_3$-based heterostructures,[1–4] culminated with the very recent discovery of superconductivity in $Nd_{0.8}Sr_{0.2}NiO_2$.[5] Bulk $NdNiO_3$ (NNO) is metallic and paramagnetic without any charge ordering (CO) and has an orthorhombic structure at room temperature.[6,7] On lowering the temperature, NNO undergoes simultaneous transitions to an insulating, antiferromagnetic, charge ordered phase having monoclinic structural symmetry. On the other hand, $LaNiO_3$ (LNO) has a rhombohedral structure and remains paramagnetic as well as metallic down to the lowest temperature.[6,7] The absence of any superconductivity in a LNO-based analogous compound ($La_{0.8}Sr_{0.2}NiO_2$)[5] with Ni in square planar oxygen coordination points toward possible strong interconnections between the electronic and magnetic phases of the parent compound and the doping induced superconductivity. In this paper, we have investigated whether an emergent antiferromagnetic, charge ordered phase can be achieved in a $LaNiO_3$ based system, which can be used to achieve unconventional superconductivity.

The heterostructure route has been shown to enable several unconventional behaviors of LNO (see Refs. 3 and 4, and references therein). For example, unlike the negligible orbital polarization of bulk LNO, the $LaNiO_3/LaTiO_3$ heterostructure exhibits strong orbital anisotropy.[8–10] Helical spin configurations were realized in LNO through the interfacial charge transfer from $La_{0.67}Sr_{0.33}MnO_3$ layers.[11] Such charge transfer can be further tuned by epitaxial strain.[12] The reduction in LNO film thickness results in an insulating phase due to the quantum confinement effect.[13–18] A ferromagnetic phase in the epitaxial LNO film on the $LaAlO_3$ (1 1 1) substrate was also demonstrated.[19] Interestingly, magnetic ordering, analogous to the E'-AFM phase and *without any charge ordering*, was obtained in two UCs (unit cells) of LNO layers sandwiched between the insulating spacer $LaAlO_3$.[16,20,21] Despite all these findings and somewhat surprisingly, long-range charge ordered

(CO), antiferromagnetic phase of LNO has not been demonstrated so far.

Apart from the abovementioned $RENiO_3/ABO_3$ ($B \neq$ Ni) heterostructures, the epitaxial growth of two different members of the $RENiO_3$ series in a layer-by-layer way offers another interesting route to achieve unconventional behaviors.[22–24] For example, bulk $EuNiO_3$ (ENO) undergoes simultaneous electronic and structural transition at 410 K and a magnetic transition around $T_N \sim 200$ K. However, the artificial structure in the form of [1 UC ENO/1 UC LNO] (UC = unit cell in pseudocubic setting) superlattice (SL) grown on single crystalline $NdGaO_3$ exhibits all four simultaneous transitions similar to bulk NNO.[22] As illustrated in Fig. 1(a), each Ni in the 1ENO/1LNO SL [marked as Ni(I)] has Eu on one side and La on the opposite side along $[0\ 0\ 1]_{pc}$, implying that each layer is equivalent to an ordered analog of the $Eu_{0.5}La_{0.5}NiO_3$ composition.[24] On the contrary, [m UC $EuNiO_3$/m UC LaNiO3] (mENO/mLNO) superlattices with $m > 1$ have additional bulk-like ENO and LNO unit cells, where each Ni has either Eu or La on both sides [respectively, marked by Ni(II) and Ni(III) in Fig. 1(b)]. Since bulk ENO and LNO have different octahedral rotational patterns $a^-a^-c^+$ vs $a^-a^-a^-$,[25,26] strong structural competition between ENO and LNO layers in these [mENO/mLNO] systems can lead to emergent electronic and magnetic phases.

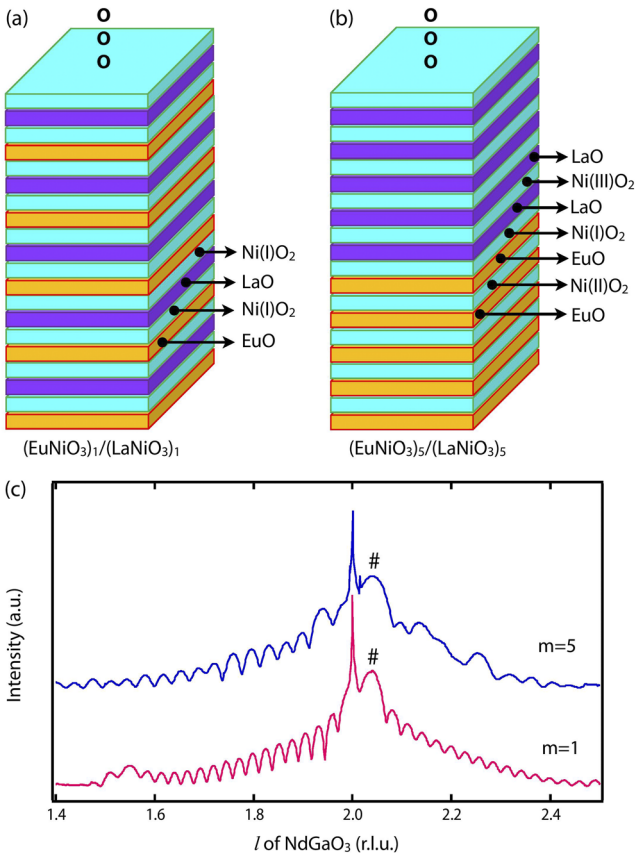

FIG. 1. Schematics of atomic planes along $[0\ 0\ 1]_{pc}$ for (a) $m = 1$ and (b) $m = 5$ samples. Ni(I)O_2 layers have EuO on one side and LaO on the opposite side. Ni(II)O_2 [Ni(III)O_2] layers have neighboring EuO [LaO] layers on both sides. (c) l-scans through $(0\ 0\ 2)_{pc}$ truncation rod. # indicates the film peak. Data have been offset along the intensity axis for visual clarity.

Here, we report the development of a new LNO-based heterostructure and demonstrate the emergence of a charge ordered antiferromagnetic insulating (AFI) phase of $LaNiO_3$. To avoid complications caused by the quantum confinement and/or interfacial charge transfer, we have judiciously built a series of [m $EuNiO_3$/m $LaNiO_3$] × N superlattices (here, N denotes the number of repeats) using pulsed laser deposition.[22–24] While the long-periodic superlattice ($m = 8$) shows entirely metallic behavior, the short-periodic superlattices undergo metal to insulator transition. Soft x-ray scattering experiments not only have found a simultaneous paramagnetic to antiferromagnetic transition but also confirmed that the magnetism is developed throughout the ENO and LNO layers. Resonant hard x-ray scattering experiments have revealed the signature of monoclinic symmetry and Ni resonance features in the metallic phase of the $m = 5$ film. The Ni resonance further increases after entering into the insulating phase, signifying the development of charge ordering throughout the whole superlattice. Magneto-transport measurements show a sign change in the Hall coefficient R_H on crossing the transition temperature in all cases, which can be explained as a consequence of Fermi surface reconstruction. The combination of advanced experimental probes has confirmed the successful creation of an antiferromagnetic, charge ordered insulating phase in LNO, which is otherwise a paramagnetic metal in the bulk form.

mENO/mLNO superlattices were grown on single crystalline $NdGaO_3$ $(1\ 1\ 0)_{or}$ [$(0\ 0\ 1)_{pc}$] (here, or and pc denote orthorhombic and pseudocubic setting, respectively) substrates using a pulsed laser deposition system.[22–24] The layer-by-layer growth of each unit cell of both ENO and LNO has been confirmed by *in situ* reflection high energy electron diffraction (not shown). For each SL, the deposition on the NGO substrate starts with an ENO layer and terminates with a LNO surface layer. The sample thickness (2 mN) is 36 UC for SLs with $m = 1$, 3, and 30 UC (32 UC) for the $m = 5$ ($m = 8$) sample. The sample quality has been checked by x-ray diffraction using a laboratory based x-ray diffractometer and also by using a six-cycle diffractometer in 6-ID-B beamline of Advanced Photon Source (APS) in Argonne National Laboratory. Magneto-transport properties of these samples have been measured in the four probe Van Der Pauw geometry using a Quantum design PPMS (Physical Property Measurement System). The issue of charge ordering in these thin films has been investigated by resonant hard x-ray scattering experiments on the Ni–K edge in 6-ID-B beam line of APS. Resonant soft x-ray scattering experiments at the Ni-L_3 edge were performed at beam line 4.0.2 of the Advanced Light Source (ALS) to probe the E'-antiferromagnetic order.

The effect of epitaxial strain of these ENO/LNO SLs has been investigated using synchrotron x-ray diffraction. Surprisingly, the effect of tensile strain in $LaNiO_3$ and $EuNiO_3$ ultra-thin films is compensated by octahedral rotations and breathing-mode distortions, instead of the expected out-of-plane compression.[26–28] Figure 1(c) shows representative diffraction scans along the $(0\ 0\ l)_{pc}$ truncation rod. As seen, the diffraction pattern of each SL consists of a sharp

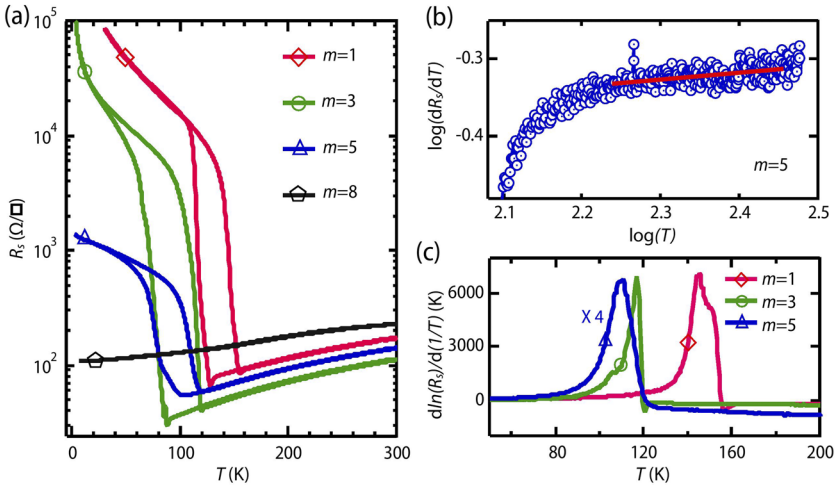

FIG. 2. (a) Sheet resistance of *m*ENO/*m*LNO SLs. All transport measurements were carried out with a temperature ramp rate of 5 K/minute. Transport data of m = 1 SL have been reproduced with permission from Middey *et al.*, Phys. Rev. Lett. **120**, 156801 (2018). Copyright 2018 American Physical Society. (b) $\log(dR_s/dT)$ vs $\log(T)$ plot for the m = 5 sample. The solid line represents a linear fitting of the experimental data. (c) Transport data of these SLs have been analyzed in terms of $d(lnR_s)/d(1/T)$ vs T plot to determine T_N.

substrate peak, a broad film peak (indicated by #), and a set of Kiessig fringes. The presence of the satellite peaks further testifies for the intended superlattice structure of each film. Surprisingly, the out-of-plane lattice constants of all of these SLs (c_{pc} = 3.793 Å, 3.793 Å, and 3.791 Å for m = 1, 3, and 5 sample, respectively) are very similar to the c_{pc} (3.8 Å) of the $EuNiO_3$ thin film on the NGO substrate.[28] This observation clearly suggests that the LNO layers follow the structural response of the ENO layers within these short-periodic superlattices. The c_{pc} of 8ENO/8LNO is slightly larger (3.807 Å), pointing toward different structural effects in the LNO layers within a long-periodic superlattice.

The modification in the electronic behavior as a function of m has been investigated by dc-transport measurements. Using a parallel resistor model with bulk-like ENO, bulk-like LNO, and the interfacial ELNO layer, the expected resistance of the SL can be expressed as

$$R_{SL} = \frac{R_{ENO}R_{LNO}R_{ELNO}}{(R_{ENO}R_{LNO} + R_{ENO}R_{ELNO} + R_{LNO}R_{ELNO})}. \quad (1)$$

Here, all NiO_2 layers in *m*ENO/*m*LNO SLs having EuO layers on both sides along $[0\ 0\ 1]_{pc}$ are named as bulk-like ENO throughout the paper. Similarly, bulk-like LNO layers refer to the NiO_2 layers with LaO layers on both sides and the interfacial ELNO layer refers to the NiO_2 layer, having EuO on one side and LaO on the other side. As expected from Eq. (1), the long-period SL (m = 8) is completely metallic [see Fig. 2(a)]. In sharp contrast, all short-periodic SLs exhibit first order MIT as a function of temperature. The transport data of m = 1 SL also show the first order MIT of the interfacial ELNO layer [marked as Ni(I) in Fig. 1]. Unexpectedly, a large change in the layer number (e.g., $m = 1 \rightarrow 5$) within each period does not result in any drastic change in the transition temperature (Table I). The observation of a MIT in the m = 5 film implies that bulk-like LNO layers marked by Ni(III) in Fig. 1(b) also become insulating below $T_{MIT} \sim 120$ K. The observation of strong thermal hysteresis signifies the spatial coexistence of metallic and insulating phases.[29–32]

Apart from the bulk LNO, the metallic phase of $RENiO_3$ shows a distinct non-Fermi liquid (NFL) behavior with the NFL exponent tunable by hydrostatic pressure or by epitaxial strain.[23,33–35] To extract the value of the power exponent n, we plot $\log(dR_s/dT)$ vs $\log(T)$ shown in Fig. 2(b), which yields $n = 1.05 \pm 0.05$, which is very close to n = 1 for $T > 175$ K for the m = 5 sample. Similar linear T-dependent behavior is also observed for the 1ENO/1LNO SL.[23] Such NFL behavior implies that the electronic behavior of LNO in these artificial structures is very different compared to the bulk LNO. The insulating phase of all $RENiO_3$ based systems hosts an E'-type antiferromagnetic phase (E'-AFM), characterized by the $(1/2\ 0\ 1/2)_{or}$ $[\equiv(1/4\ 1/4\ 1/4)_{pc}]$ magnetic wave vector.[36] A reliable estimate of the magnetic transition temperature (T_N) can be obtained from resistivity analysis.[37,38] The $d(lnR_s)/d(1/T)$ vs T plot [Fig. 2(c)] yields T_N of 145 K, 115 K, and 110 K for SLs with m = 1, 3, and 5 SL, respectively, illustrating simultaneous electronic and magnetic transitions of these superlattices.

Simultaneous MIT and paramagnetic to E'-AFM transition for m = 1 SL were also confirmed by our earlier resonant soft x-ray diffraction (RSXD) experiments with the photon energy tuned to 852 eV.[22] Such a RSXD technique has been demonstrated as a very effective way to investigate the E'-AFM phase of various $RENiO_3$ thin films and heterostructures.[20,22,24,34,39–43] As shown in Fig. 3(a), a $(1/4\ 1/4\ 1/4)_{pc}$ diffraction peak is also observed at 50 K in RSXD of m = 5 SL, which vanishes gradually with increasing T. A plot of the area under this peak as a function of T gives $T_N \sim 115 \pm 5$ K [see Fig. 3(b)], which is very close to the values of T_N obtained from our transport data shown in Fig. 2(c). Thus, apart from the

TABLE I. Summary of transport data (heating run).

m	T_{MIT} (K)	T_N (K)	NFL exponent (n)
1	155	145	1 for $T > 180$ K
3	120	115	1 for $T > 240$ K
5	120	110	1 for $T > 175$ K

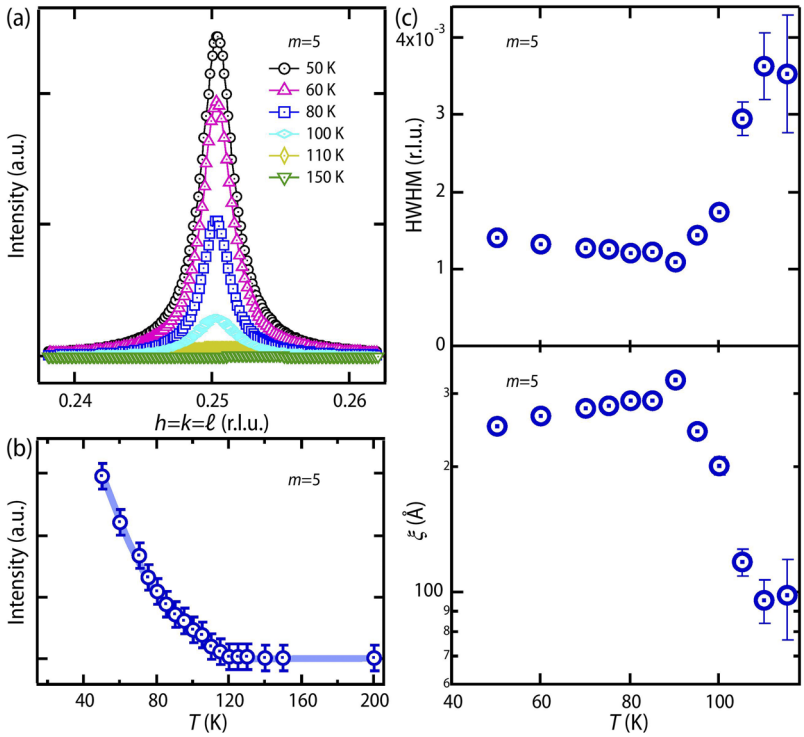

FIG. 3. (a) Measured magnetic scattering for the $m = 5$ sample at different temperatures. The integrated intensity of this peak has been plotted as a function of T in panel (b). (c) Temperature dependence of the HWHM of the peak (upper panel) and the magnetic correlation length (lower panel).

interfacial unit cells, bulk-like LNO layers also undergo simultaneous metal–insulator and paramagnetic–antiferromagnetic transitions in such heterostructures. The temperature dependence of the Lorentzian half width at half maximum (HWHM) of the E'-AFM peak is plotted in the upper panel of Fig. 3(c). The magnetic correlation length along the $[1\ 1\ 1]_{pc}$ direction, $\xi = a_{NGO}/[2\sqrt{3}\pi^{*}\text{HWHM}]$ is approximately 285 Å up to 90 K [lower panel of Fig. 3(c)], which is larger than the film thickness along the $[1\ 1\ 1]_{pc}$ direction. This finding establishes that the E'-antiferromagnetic spin arrangement is developed throughout the entire sample, including the bulk-like LNO layers.

The microscopic origin of the simultaneous electronic and magnetic transitions in $RENiO_3$ can be accounted by the hole-Fermi surface nesting driven spin-density wave (SDW) transition.[20,40,44,45] The consequence of nesting driven transition in multi-band nickelates can be captured by measuring the Hall coefficient (R_H) as a function of temperature.[38] For example, the previous measurements of R_H[38] reveal that R_H, dominated by the contribution from large hole pockets, is positive in the paramagnetic metallic phase and becomes negative below the SDW transition as the remaining small electron pockets contribute to R_H in the antiferromagnetic insulating phase. Figures 4(a) and 4(b) show the variation of transverse resistance (R_{xy}) as a function of the applied magnetic field (H) after antisymmetrization[38] for the m = 3 and m = 5 SLs, respectively. These measurements were performed in the cooling run. As shown in Fig. 4(a), the positive slope of the curves R_H ($=tdR_{xy}/dH$, t = film thickness) is hole-like above 100 K for the $m = 3$ sample and then becomes electron-like. For the $m = 5$ film, R_H is also hole-like down to 120 K and is completely electron-like at 80 K. In the intermediate temperature range around 100 K, R_{xy} shows a non-linear behavior with H and switches from the electron-to hole-like behavior with increasing H. Such a small value of R_{xy} indicates that the difference in volume between electron and hole pockets is very small at that temperature. Similar switching of R_H was also observed in the 1ENO/1LNO SL (not shown). The crossover of R_H in the vicinity of $T_{MIT} \sim T_N$ strongly suggests a SDW driven origin of the antiferromagnetic insulating (AFI) phase of these ENO/LNO superlattices.

After confirming the simultaneous electronic and magnetic transitions in SLs, we investigated the issue of the highly debated charge ordering. Unlike the bulk samples, thin films can host an insulating phase without any CO.[22,40,43,46] The conventional picture of charge disproportionation (CD) on Ni ions ($d^7+d^7 \rightarrow d^{7+\delta} + d^{7-\delta}$)[40,47–51] is also challenged by the alternative mechanism of the bond disproportion (BD) transition, specially proposed for the most distorted members of the series.[52–56] Such BD transition ($d^8\underline{L}+d^8\underline{L} \rightarrow d^8 + d^8\underline{L}^2$, $\underline{L}$ represents a hole on oxygen) results in a rocksalt-type pattern with alternating NiO_6 octahedra with d^8 having long-bond (LB) and $d^8\underline{L}^2$ having short-bond (SB). Most importantly, the results of x-ray absorption spectroscopy and x-ray scattering experiments, conventionally used to conclude CD on Ni sublattices[48–50,57,58] can be also accounted by the BD transition.[21,56,59,60] However, a larger amount of BD can generate a significant amount of Ni e_g charge disproportionation. For example, double cluster calculation with a BD of $\delta d \sim 0.2$ Å by Green *et al.*[59] has not only obtained unequal spin values ($S \sim 1.0$ and 0.1 on LB and SB sites, respectively) but also a difference of ~0.3e in the e_g electronic occupancy between LB and SB sites. It is important to note that

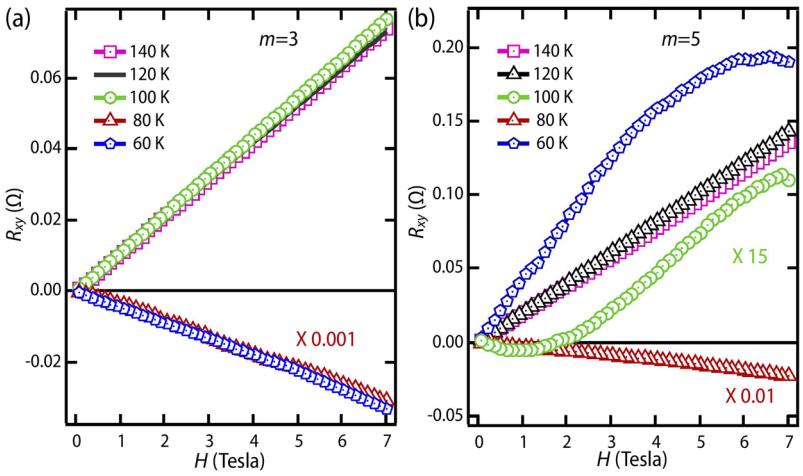

FIG. 4. Transverse resistance R_{xy} as a function of H at different T for the (a) m = 3 and (b) m = 5 samples. R_{xy} of selected datasets are scaled and indicated by scaling factors.

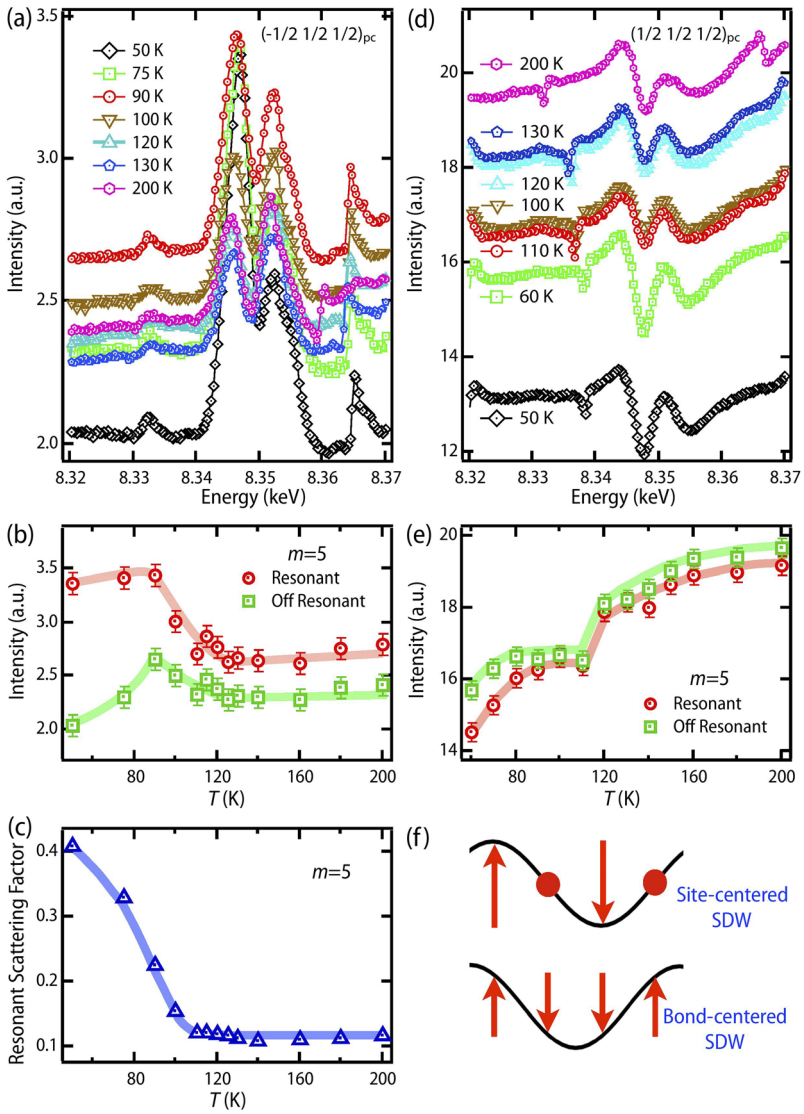

FIG. 5. Resonance energy scan of the m = 5SL at various temperatures for (a) $(-1/2\ 1/2\ 1/2)_{pc}$ and (d) $(1/2\ 1/2\ 1/2)_{pc}$ Bragg peaks. Temperature dependence of the corresponding resonant intensity (I_{res}) and the off-resonant intensity (I_{offres}) are plotted in (b) and (e). (c) Variation of the resonance enhancement factor $(\sqrt{I_{res}} - \sqrt{I_{offres}})$ for the $(-1/2\ 1/2\ 1/2)_{pc}$ peak with T. (f) Site-centered SDW with charge ordering vs bond-centered SDW without charge ordering.[44]

the amount of CD, obtained experimentally, is of the same order $2\delta \sim 0.45e$.[48] This implies BD and CD are cooperative in nature for bulk rare-earth nickelates. On the other hand, Lee *et al.* have shown that CD on Ni sublattices can be realized as a simple consequence of the SDW transition.[44,45]

In order to investigate BD/CD in the weakly insulating phase of the $m = 5$ film, we have measured resonant x-ray scattering at the Ni–K edge ($1s \rightarrow 4p$) around $(0\ 1\ 1)_{or}$ [$\equiv(-1/2\ 1/2\ 1/2)_{pc}$] and $(1\ 0\ 1)_{or}$ [$\equiv(1/2\ 1/2\ 1/2)_{pc}$] reflections.[21,22,48–50] The details of the energy and momentum dependence of these diffraction peaks are given in Ref. 61. Here, we note that the $(-1/2\ 1/2\ 1/2)_{pc}$ peak is allowed for monoclinic and forbidden for orthorhombic symmetry. On the other hand, the $(1/2\ 1/2\ 1/2)_{pc}$ reflection is allowed in both monoclinic and orthorhombic phases, but both of these reflections are forbidden for rhombohedral symmetry. As shown in Fig. 5(a), the $m = 5$ sample exhibits a resonance feature for the $(-1/2\ 1/2\ 1/2)_{pc}$ diffraction peak around 8.345 keV photon energy at 50 K. Generally, both the resonant intensity (I_{res}) and the off-resonant intensity (I_{offres}) decrease with the increase of T as previously reported for the insulating phase of the thick $NdNiO_3$ film and for the 1ENO/1LNO SL.[21,22,48] However, I_{offres} increases strongly up to 90 K for $m = 5$ SL [Fig. 5(b)] suggesting the existence of additional structural effects below 90 K. Furthermore, both I_{res} and I_{offres} decrease above 90 K, where the magnetic correlation length also decreases. This strongly implies strong interconnection between charge ordering and magnetic ordering. Interestingly, I_{res} is also non-zero in the metallic phase and the line shape is very similar to the resonant line shape observed in the insulating phase of the $EuNiO_3$ thin film.[42] The resonance and off-resonance intensities for the $(1/2\ 1/2\ 1/2)_{pc}$ diffraction peak increase up to 90 K and shows a marked jump across the insulator to metal transition [see Figs. 5(d) and 5(e)]. The observation of both $(-1/2\ 1/2\ 1/2)_{pc}$ and $(1/2\ 1/2\ 1/2)_{pc}$ reflections and Ni resonance in the metallic phase of the SL clearly establishes the presence of strong monoclinic distortion in the metallic phase of the $m = 5$ SL. Moreover, the temperature dependence of the resonance enhancement factor $[\sqrt{I}_{res} - \sqrt{I}_{offres}]$ for the $(-1/2\ 1/2\ 1/2)_{pc}$ diffraction peak [Fig. 5(c)] demonstrates the onset of a CO transition around 110 K.

From these experimental results, we suggest the following scenario for simultaneous metal–insulator, CO, and magnetic transitions in these SLs. As shown in Fig. 1(a), $m = 1$ SL consists of only interfacial Nis, having EuO on one side and LaO layers on the opposite side. The site-centered type SDW transition [Fig. 5(f)] in all of these interfacial layers can give rise to the AFI phase with CO. Apart from the interfacial NiO_2 layers, $m = 5$ SL also contain bulk-like ENO and bulk-like LNO layers. The interfacial layers and the bulk-like LNO layers remain metallic down to 120 K and the bulk-like ENO layers are bond ordered insulators with monoclinic symmetry, resulting in the overall metallic behavior of the sample. In addition to the interfacial layers, bulk-like LNO layers also undergo the SDW transition to develop the antiferromagnetic, charge ordered, insulating phase throughout the 5ENO/5LNO sample. Unlike the pure SDW phase without CO obtained in the $LaNiO_3/LaAlO_3$ SL through dimensionality control,[16,20,21] $LaNiO_3$ layers in the present study undergo the SDW transition in spite of the presence of three dimensional NiO_6 octahedral networks, resulting in this emergent charge ordered, antiferromagnetic phase of $LaNiO_3$, which is unattainable in the bulk.

To summarize, our detailed measurements, including magneto-transport, hard x-ray resonant scattering, and soft x-ray resonant magnetic scattering, have found simultaneous metal–insulator, charge ordering, and magnetic transitions in these $(EuNiO_3)_m/(LaNiO_3)_m$ SLs. Moreover, these measurements demonstrated strong interrelation between the spin and charge orders. In addition, the Hall coefficient shows crossover from the hole-like to electron-like behavior across the transitions. All of these experimental observations can be successfully accounted by the notion of Fermi surface nesting emerging in the bulk-like LNO layers and the interfacial layer. The emergent antiferromagnetic, charge ordered phase of $LaNiO_3$ can be explored as a parent compound to achieve high T_c superconductivity.

S.M. acknowledges the DST Nano Mission, Grant No. DST/NM/NS/2018/246, and the SERB Early Career Research Award (Grant No. ECR/2018/001512) for financial support. S.M. also acknowledges support from Infosys Foundation, Bangalore. J.C. was supported by the Gordon and Betty Moore Foundation EPiQS Initiative through Grant No. GBMF4534. X.L. was supported by the Department of Energy under Grant No. DE-SC0012375. This research used resources of the Advanced Photon Source, a U.S. Department of Energy Office of Science User Facility operated by Argonne National Laboratory under Contract No. DE-AC02-06CH11357. This research used resources of the Advanced Light Source, which is a Department of Energy Office of Science User Facility under Contract No. DE-AC02-05CH11231.

REFERENCES

[1] J. c. v. Chaloupka and G. Khaliullin, Phys. Rev. Lett. **100**, 016404 (2008).
[2] P. Hansmann, X. Yang, A. Toschi, G. Khaliullin, O. K. Andersen, and K. Held, Phys. Rev. Lett. **103**, 016401 (2009).
[3] S. Middey, J. Chakhalian, P. Mahadevan, J. W. Freeland, A. J. Millis, and D. D. Sarma, Annu. Rev. Mater. Res. **46**, 305 (2016).
[4] S. Catalano, M. Gibert, J. Fowlie, J. Íñiguez, J.-M. Triscone, and J. Kreisel, Rep. Prog. Phys. **81**, 046501 (2018).
[5] D. Li, K. Lee, B. Y. Wang, M. Osada, S. Crossley, H. R. Lee, Y. Cui, Y. Hikita, and H. Y. Hwang, Nature **572**, 624 (2019).
[6] M. L. Medarde, J. Phys.: Condens. Matter **9**, 1679 (1997).
[7] G. Catalan, Phase Transitions **81**, 729 (2008).
[8] H. Chen, A. J. Millis, and C. A. Marianetti, Phys. Rev. Lett. **111**, 116403 (2013).
[9] A. S. Disa, D. P. Kumah, A. Malashevich, H. Chen, D. A. Arena, E. D. Specht, S. Ismail-Beigi, F. J. Walker, and C. H. Ahn, Phys. Rev. Lett. **114**, 026801 (2015).
[10] Y. Cao, X. Liu, M. Kareev, D. Choudhury, S. Middey, D. Meyers, J. Kim, P. Ryan, J. Freeland, and J. Chakhalian, Nat. Commun. **7**, 10418 (2016).
[11] J. D. Hoffman, B. J. Kirby, J. Kwon, G. Fabbris, D. Meyers, J. W. Freeland, I. Martin, O. G. Heinonen, P. Steadman, H. Zhou, C. M. Schlepütz, M. P. M. Dean, S. G. E. te Velthuis, J.-M. Zuo, and A. Bhattacharya, Phys. Rev. X **6**, 041038 (2016).
[12] Z. Xu, S. Hu, R. Wu, J.-O. Wang, T. Wu, and L. Chen, ACS Appl. Mater. Interfaces **10**, 30803–30810 (2018).
[13] J. Liu, S. Okamoto, M. van Veenendaal, M. Kareev, B. Gray, P. Ryan, J. W. Freeland, and J. Chakhalian, Phys. Rev. B **83**, 161102 (2011).
[14] J. W. Freeland, J. Liu, M. Kareev, B. Gray, J. W. Kim, P. Ryan, R. Pentcheva, and J. Chakhalian, Europhys. Lett. **96**, 57004 (2011).
[15] R. Scherwitzl, S. Gariglio, M. Gabay, P. Zubko, M. Gibert, and J.-M. Triscone, Phys. Rev. Lett. **106**, 246403 (2011).
[16] A. V. Boris, Y. Matiks, E. Benckiser, A. Frano, P. Popovich, V. Hinkov, P. Wochner, M. Castro-Colin, E. Detemple, V. K. Malik, C. Bernhard, T. Prokscha, A. Suter, Z. Salman, E. Morenzoni, G. Cristiani, H. U. Habermeier, and B. Keimer, Science **332**, 937 (2011).

[17]P. D. C. King, H. I. Wei, Y. F. Nie, M. Uchida, C. Adamo, S. Zhu, X. He, I. Božović, D. G. Schlom, and K. M. Shen, Nat. Nanotechnol. **9**, 443 (2014).
[18]A. M. Kaiser, A. X. Gray, G. Conti, J. Son, A. Greer, A. Perona, A. Rattanachata, A. Y. Saw, A. Bostwick, S. Yang, S.-H. Yang, E. M. Gullikson, J. B. Kortright, S. Stemmer, and C. S. Fadley, Phys. Rev. Lett. **107**, 116402 (2011).
[19]T. Asaba, Z. Xiang, T. H. Kim, M. S. Rzchowski, C. B. Eom, and L. Li, Phys. Rev. B **98**, 121105 (2018).
[20]A. Frano, E. Schierle, M. W. Haverkort, Y. Lu, M. Wu, S. Blanco-Canosa, U. Nwankwo, A. V. Boris, P. Wochner, G. Cristiani, H. U. Habermeier, G. Logvenov, V. Hinkov, E. Benckiser, E. Weschke, and B. Keimer, Phys. Rev. Lett. **111**, 106804 (2013).
[21]Y. Lu, A. Frano, M. Bluschke, M. Hepting, S. Macke, J. Strempfer, P. Wochner, G. Cristiani, G. Logvenov, H.-U. Habermeier, M. W. Haverkort, B. Keimer, and E. Benckiser, Phys. Rev. B **93**, 165121 (2016).
[22]S. Middey, D. Meyers, M. Kareev, Y. Cao, X. Liu, P. Shafer, J. W. Freeland, J.-W. Kim, P. J. Ryan, and J. Chakhalian, Phys. Rev. Lett. **120**, 156801 (2018).
[23]S. Middey, D. Meyers, M. Kareev, X. Liu, Y. Cao, J. W. Freeland, and J. Chakhalian, Phys. Rev. B **98**, 045115 (2018).
[24]S. Middey, D. Meyers, R. Kumar Patel, X. Liu, M. Kareev, P. Shafer, J.-W. Kim, P. J. Ryan, and J. Chakhalian, Appl. Phys. Lett. **113**, 081602 (2018).
[25]A. M. Glazer, Acta Crystallogr., Sect. B **28**, 3384 (1972).
[26]I. C. Tung, P. V. Balachandran, J. Liu, B. A. Gray, E. A. Karapetrova, J. H. Lee, J. Chakhalian, M. J. Bedzyk, J. M. Rondinelli, and J. W. Freeland, Phys. Rev. B **88**, 205112 (2013).
[27]J. Chakhalian, J. M. Rondinelli, J. Liu, B. A. Gray, M. Kareev, E. J. Moon, N. Prasai, J. L. Cohn, M. Varela, I. C. Tung, M. J. Bedzyk, S. G. Altendorf, F. Strigari, B. Dabrowski, L. H. Tjeng, P. J. Ryan, and J. W. Freeland, Phys. Rev. Lett. **107**, 116805 (2011).
[28]D. Meyers, S. Middey, M. Kareev, M. van Veenendaal, E. J. Moon, B. A. Gray, J. Liu, J. W. Freeland, and J. Chakhalian, Phys. Rev. B **88**, 075116 (2013).
[29]G. N. Daptary, S. Kumar, M. Kareev, J. Chakhalian, A. Bid, and S. Middey, Phys. Rev. B **100**, 125105 (2019).
[30]D. Preziosi, L. Lopez-Mir, X. Li, T. Cornelissen, J. H. Lee, F. Trier, K. Bouzehouane, S. Valencia, A. Gloter, A. Bibes *et al.*, Nano Lett. **18**, 2226 (2018).
[31]J. F. Ding, K. X. Jin, Z. Zhang, and T. Wu, Appl. Phys. Lett. **100**, 062402 (2012).
[32]J. Ding, Z. Lin, J. Wu, Z. Dong, and T. Wu, Small **11**, 576 (2015).
[33]J.-S. Zhou, J. B. Goodenough, and B. Dabrowski, Phys. Rev. Lett. **94**, 226602 (2005).
[34]J. Liu, M. Kargarian, M. Kareev, B. Gray, P. J. Ryan, A. Cruz, N. Tahir, Y.-D. Chuang, J. Guo, J. M. Rondinelli, J. W. Freeland, G. A. Fiete, and J. Chakhalian, Nat. Commun. **4**, 2714 (2013).
[35]E. Mikheev, A. J. Hauser, B. Himmetoglu, N. E. Moreno, A. Janotti, C. G. Van de Walle, and S. Stemmer, Sci. Adv. **1**, e1500797 (2015).
[36]J. L. García-Muñoz, J. Rodríguez-Carvajal, and P. Lacorre, Phys. Rev. B **50**, 978 (1994).
[37]J.-S. Zhou, J. B. Goodenough, and B. Dabrowski, Phys. Rev. Lett. **95**, 127204 (2005).
[38]S. K. Ojha, S. Ray, T. Das, S. Middey, S. Sarkar, P. Mahadevan, Z. Wang, Y. Zhu, X. Liu, M. Kareev, and J. Chakhalian, Phys. Rev. B **99**, 235153 (2019).
[39]V. Scagnoli, U. Staub, A. M. Mulders, M. Janousch, G. I. Meijer, G. Hammerl, J. M. Tonnerre, and N. Stojic, Phys. Rev. B **73**, 100409 (2006).
[40]M. Hepting, M. Minola, A. Frano, G. Cristiani, G. Logvenov, E. Schierle, M. Wu, M. Bluschke, E. Weschke, H.-U. Habermeier, E. Benckiser, M. Le Tacon, and B. Keimer, Phys. Rev. Lett. **113**, 227206 (2014).
[41]S. Catalano, M. Gibert, V. Bisogni, O. E. Peil, F. He, R. Sutarto, M. Viret, P. Zubko, R. Scherwitzl, A. Georges, G. A. Sawatzky, T. Schmitt, and J.-M. Triscone, APL Mater. **2**, 116110 (2014).
[42]D. Meyers, S. Middey, M. Kareev, J. Liu, J. W. Kim, P. Shafer, P. J. Ryan, and J. Chakhalian, Phys. Rev. B **92**, 235126 (2015).
[43]D. Meyers, J. Liu, J. W. Freeland, S. Middey, M. Kareev, J. Kwon, J. M. Zuo, Y.-D. Chuang, J. W. Kim, P. J. Ryan *et al.*, Sci. Rep. **6**, 27934 (2016).
[44]S. Lee, R. Chen, and L. Balents, Phys. Rev. Lett. **106**, 016405 (2011).
[45]S. Lee, R. Chen, and L. Balents, Phys. Rev. B **84**, 165119 (2011).
[46]M. H. Upton, Y. Choi, H. Park, J. Liu, D. Meyers, J. Chakhalian, S. Middey, J.-W. Kim, and P. J. Ryan, Phys. Rev. Lett. **115**, 036401 (2015).
[47]J. A. Alonso, J. L. García-Muñoz, M. T. Fernández-Díaz, M. A. G. Aranda, M. J. Martínez-Lope, and M. T. Casais, Phys. Rev. Lett. **82**, 3871 (1999).
[48]U. Staub, G. I. Meijer, F. Fauth, R. Allenspach, J. G. Bednorz, J. Karpinski, S. M. Kazakov, L. Paolasini, and F. d'Acapito, Phys. Rev. Lett. **88**, 126402 (2002).
[49]J. E. Lorenzo, J. L. Hodeau, L. Paolasini, S. Lefloch, J. A. Alonso, and G. Demazeau, Phys. Rev. B **71**, 045128 (2005).
[50]V. Scagnoli, U. Staub, M. Janousch, A. M. Mulders, M. Shi, G. I. Meijer, S. Rosenkranz, S. B. Wilkins, L. Paolasini, J. Karpinski, S. M. Kazakov, and S. W. Lovesey, Phys. Rev. B **72**, 155111 (2005).
[51]I. I. Mazin, D. I. Khomskii, R. Lengsdorf, J. A. Alonso, W. G. Marshall, R. M. Ibberson, A. Podlesnyak, M. J. Martínez-Lope, and M. M. Abd-Elmeguid, Phys. Rev. Lett. **98**, 176406 (2007).
[52]T. Mizokawa, D. I. Khomskii, and G. A. Sawatzky, Phys. Rev. B **61**, 11263 (2000).
[53]H. Park, A. J. Millis, and C. A. Marianetti, Phys. Rev. Lett. **109**, 156402 (2012).
[54]S. Johnston, A. Mukherjee, I. Elfimov, M. Berciu, and G. A. Sawatzky, Phys. Rev. Lett. **112**, 106404 (2014).
[55]A. Subedi, O. E. Peil, and A. Georges, Phys. Rev. B **91**, 075128 (2015).
[56]K. Haule and G. L. Pascut, Sci. Rep. **7**, 2045 (2017).
[57]C. Piamonteze, F. M. F. de Groot, H. C. N. Tolentino, A. Y. Ramos, N. E. Massa, J. A. Alonso, and M. J. Martínez-Lope, Phys. Rev. B **71**, 020406 (2005).
[58]J. W. Freeland, M. van Veenendaal, and J. Chakhalian, J. Electron Spectrosc. Relat. Phenom. **208**, 56 (2016), special issue: Electronic structure and function from state-of-the-art spectroscopy and theory.
[59]R. J. Green, M. W. Haverkort, and G. A. Sawatzky, Phys. Rev. B **94**, 195127 (2016).
[60]M. Hepting, R. J. Green, Z. Zhong, M. Bluschke, Y. E. Suyolcu, S. Macke, A. Frano, S. Catalano, M. Gibert, R. Sutarto *et al.*, Nat. Phys. **14**, 1097 (2018).
[61]We recap that the scattering intensities of $(0\,1\,1)_{or}$ and $(1\,0\,1)_{or}$ peaks are given by

$$I_{011}(\mathbf{Q},E) \propto \left[A^2_{\mathrm{O,RE}}(\mathbf{Q}) + 2A_{\mathrm{O,RE}}(\mathbf{Q}).2\left(\Delta f^0_{\mathrm{Ni}}(\mathbf{Q}) + \Delta f'_{\mathrm{Ni}}(E) + \Delta f''_{\mathrm{Ni}}(E)\right) + 4\left(\Delta f^0_{\mathrm{Ni}}(\mathbf{Q}) + \Delta f'_{\mathrm{Ni}}(E) + \Delta f''_{\mathrm{Ni}}(E)\right)^2\right],$$

$$I_{101}(\mathbf{Q},E) \propto \left[B^2_{\mathrm{O,RE}}(\mathbf{Q}) - 2B_{\mathrm{O,RE}}(\mathbf{Q}).2\left(\Delta f^0_{\mathrm{Ni}}(\mathbf{Q}) + \Delta f'_{\mathrm{Ni}}(E) + \Delta f''_{\mathrm{Ni}}(E)\right) + 4\left(\Delta f^0_{\mathrm{Ni}}(\mathbf{Q}) + \Delta f'_{\mathrm{Ni}}(E) + \Delta f''_{\mathrm{Ni}}(E)\right)^2\right],$$

with $\Delta f^0_{\mathrm{Ni}}(\mathbf{Q}) = [f^0_{\mathrm{Ni1}}(\mathbf{Q}) - f^0_{\mathrm{Ni2}}(\mathbf{Q})]$, $\Delta f'_{\mathrm{Ni}}(\mathrm{E}) = [f'_{\mathrm{Ni1}}(\mathrm{E}) - f'_{\mathrm{Ni2}}(\mathrm{E})]$, and $\Delta f''_{\mathrm{Ni}}(E) = [f''_{\mathrm{Ni1}}(E) - f''_{\mathrm{Ni2}}(E)]$.[22] $\mathrm{A_{O,RE}}(\mathbf{Q})$ and $\mathrm{B_{O,RE}}(\mathbf{Q})$ represent the energy-independent Thompson scattering (TS) terms for the RE and O sites and $f^0_{\mathrm{Ni}}(\mathbf{Q})$ corresponds to the TS term for the Ni sites. $f'_{\mathrm{Ni}}(\mathrm{E})$ and $f''_{\mathrm{Ni}}(E)$ term, responsible for the resonance behavior, are the real and imaginary energy-dispersive correction factors. Since $f'_{\mathrm{Ni}}(\mathrm{E})$ and $f''_{\mathrm{Ni}}(E)$ are negligibly away from the resonance, the off-resonant intensity represents pure structural information. The energy-independent terms $\mathrm{A_{O,RE}}$ and $\mathrm{B_{O,RE}}$ can also result in energy dependent features at the resonance energy due to their coupling with the energy dependent terms $\Delta f'_{\mathrm{Ni}}$ and $\Delta f''_{\mathrm{Ni}}$. The minus sign in the last equation implies that the resonance feature around 8.345 keV would appear as a dip for the $(1\,0\,1)_{or}$ diffraction peak. We also note that the off-resonance intensity of $(1\,0\,1)_{or}$ will be stronger compared to the $(0\,1\,1)_{or}$ peak due to the strong structural contribution via the $\mathrm{B_{O,RE}}$ term in the last equation.